MATERIALS CHEMISTRY FRONTIERS

RESEARCH ARTICLE

View Article Online
View Journal | View Issue

Cite this: *Mater. Chem. Front.*, 2023, **7**, 2671

Received 24th January 2023,
Accepted 29th March 2023

DOI: 10.1039/d3qm00091e

rsc.li/frontiers-materials

Electrofabrication of a low molecular weight hydrogel at high pH†

Courtenay Patterson,[a] Santanu Panja,[a] Wanli Liu,[b] Andrew R. Mount,[c] Adam Squires[b] and Dave J. Adams*[a]

Fmoc-3 is a low-molecular-weight gelator that self-assembles to form hydrogels at basic pH. Here, using Fmoc-3, we show the first electrodeposition at high pH of a low molecular weight gelator using an electrochemically generated pH gradient. We also show that electrodeposition can be used to grow simultaneously two hydrogels at opposing pH extremes on different electrodes.

Electrodeposition is an electrochemical process that can be used to assemble solid or soft materials on electrode surfaces.[1–4] This technique has been used to form hydrogels, triggering the self-assembly of gelling molecules or polymers upon application of a current or electric field. Hydrogels have been fabricated using this method from small molecule gelators such as dipeptides,[5] dibenzoyl cystine and functionalised amino acids.[6] Polymeric systems such as collagen,[7] chitosan,[8,9] silk[10] and alginate[11,12] have also been used to form gels using this approach.

To fabricate pH-sensitive hydrogels from gelator solutions, electrodeposition can be used through generating localised pH gradients at electrode surfaces by exploiting various electrochemical acid–base reactions, which could be induced by reduction–oxidation reactions.[2,13,14] Here, electrodes are placed with bulk solutions of the soluble gelling agent. Current is then passed between the working and a counter electrode, leading through electrochemical reaction to, for example a change in pH at the working electrode. A localised region of pH change then develops at the electrode which leads to the charge being removed there from the gelator structure through protonation/deprotonation, the loss of electrostatic repulsion, and hence the self-assembly of the gelator to form a gel on the electrode surface. It should be noted that no gelation occurs in the bulk solution, giving excellent spatiotemporal control over gelation. Depending on the system or additives used, the application of a constant current can result in the diffusion of hydrogen or hydroxyl ions from the electrode surface, creating a significantly more acidic or basic pH zone than the bulk solution. The size of this zone, and so the size of the hydrogel, is governed by the diffusion distance of the hydrogen or hydroxyl ions.[5] For low molecular weight gelators (LMWG), electrodeposition has been used to form gels at low pH, typically by exploiting the hydroquinone–quinone couple[5,15] or the direct oxidation of water.[16]

Gelling at high pH by electrodeposition is yet to be described for a LMWG. However, gelling at high pH has been achieved for chitosan (a biopolymer containing many charged ammonium ions at neutral pH) by the galvanostatic reduction of hydrogen peroxide (Fig. 1b). Gels formed using LMWG have significantly different properties to gels formed from biopolymers. Gels formed from LMWG can be formed at significantly lower concentration of gelating agent, can be significantly stiffer, break at significantly lower strain and can more quickly be broken down since the constituent gelling molecules are of

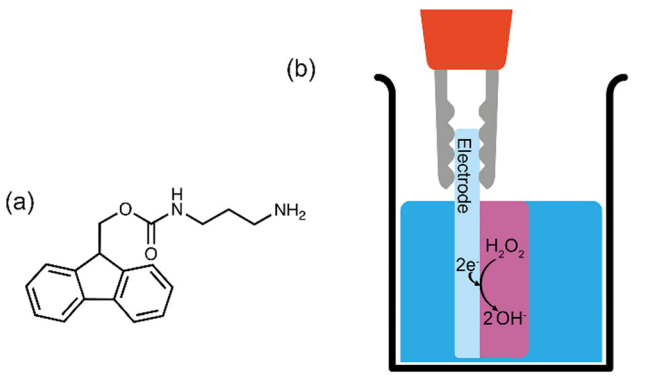

Fig. 1 (a) Chemical structure of the LMWG Fmoc-3 (b) Schematic representation of the electrochemical gelation of Fmoc-3 *via* the two-electron, electrochemical reduction of hydrogen peroxide, producing two hydroxide ions. In this case, the electrode represents a flat glass FTO slide.

[a] *School of Chemistry, University of Glasgow, Glasgow, G12 8QQ, UK. E-mail: dave.adams@glasgow.ac.uk*
[b] *Department of Chemistry, University of Bath, Bath, BA2 7AX, UK*
[c] *EastCHEM, School of Chemistry, University of Edinburgh, EH9 3FJ, UK*

† Electronic supplementary information (ESI) available. See DOI: https://doi.org/10.1039/d3qm00091e

much lower mass. Hence such gels are complementary to those formed using polymeric gelator.

During the electrochemical reduction of hydrogen peroxide, hydroxide ions are produced at the electrode-solution interface, creating a basic pH zone.[14] This results in deprotonation of the ammonium groups in this zone, decreasing chitosan's solubility to induce gelation at the electrode surface.[8] Electrodeposition of chitosan has also been achieved through the electrolysis of water, which produces hydroxide ions and hydrogen gas at the cathode surface.[17] Although the production of hydroxide ions increases the local pH to induce gelation, water electrolysis is often avoided for longer deposition times due to the production of hydrogen gas bubbles that perforate through the hydrogel surface.[17]

Here, we show how electrodeposition at high pH can be applied to a LMWG system. We then show the simultaneous formation of two low molecular weight hydrogels at acidic and basic pH extremes by coupling an anodic and cathodic neutralisation method. Gelling at higher pH complements the work carried out for low pH gels, and also opens up possibilities where gelation can occur at, or close to physiological pH,[14] as well as being of potential use within dissipative systems.[18]

Fmoc-3 (Fig. 1a; mono-Fmoc 1,3-diaminopropane hydrochloride) is an effective LMWG. To form a hydrogel, the gelator molecules self-assemble in water to form fibrous structures that entangle when the pH of the solution is raised above the pK_a (8.4–8.7).[19] Previous work has shown that this can be achieved chemically *via* the autocatalytic reaction of urea and urease to produce ammonia, which results in an increase in the pH.[19]

To now electrochemically gel Fmoc-3, 7 mL solutions of Fmoc-3 (5 mg mL^{-1} in aq. NaCl 0.1 M) were prepared to give gelator solutions at a pH of 6.5. As carbon dioxide in the atmosphere readily dissolves in water to give dissolved CO_2, carbonic acid and the bicarbonate anion, it is likely that the pH is fixed at 6.5, within the range of the apparent pK_a value of this system[20] due to the natural buffering of these dissolved carbon dioxide species in the gelator solutions. To create the basic pH gradient at the electrode surface, 70 μL of hydrogen peroxide solution was added to the Fmoc-3 solutions immediately prior to gelation. The importance of hydrogen peroxide reduction on hydrogel formation was investigated by growing Fmoc-3 hydrogels in the absence of hydrogen peroxide and in the presence of hydrogen peroxide (adding 70 μL aliquots of hydrogen peroxide solutions at concentrations of 1 M to 4 M). In the absence of hydrogen peroxide, the gelation process relies on the electrochemical reduction of water which produces hydrogen gas as a by-product.

To grow the Fmoc-3 hydrogels, a three-electrode set-up under galvanostatic control consisted of an FTO glass slide (working electrode), platinum wire (counter electrode) and Ag/AgCl (reference electrode) (Fig. S2, ESI†). A current density of −0.7 mA cm^{-2} was found to be satisfactory for gel growth and was applied to all Fmoc-3 gelator solutions for 900 seconds (Fig. 2f). In the absence of hydrogen peroxide and across the entire hydrogen peroxide concentration range, hydrogel formation was observed at the working electrode surface (Fig. 2 and Fig. S3, ESI†).

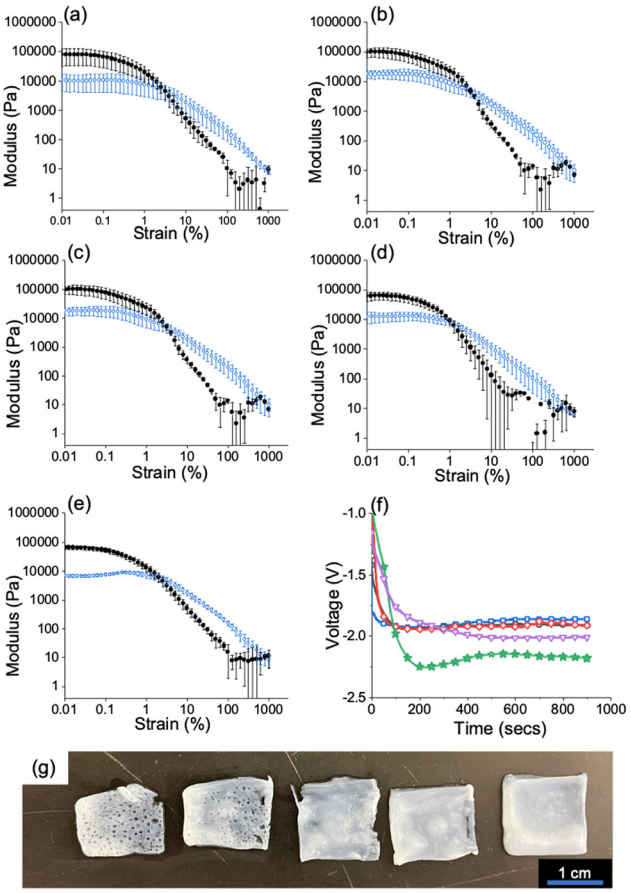

Fig. 2 (a–e) Strain sweeps showing storage (G') and loss moduli (G'') (a) In the absence of hydrogen peroxide and at various concentrations of hydrogen peroxide (b) 1 M (c) 2 M (d) 3 M (e) 4 M. Full rheology data can be found in the ESI† (Fig. S9). For all gels, G' = black/filled circle data, G'' = blue data/hollow circle data. All measurements were performed in triplicate and errors were calculated from the standard deviation. (f) chronopotentiometry data for hydrogels grown (a) in the absence of hydrogen peroxide (green/star data) and when 70 μL of 1 M (pink/triangle data), 2 M (red/diamond data), 3 M (black/circle data) and 4 M (blue/square data) hydrogen peroxide solution (g) Images of Fmoc-3 hydrogels grown (a) in the absence of hydrogen peroxide (far left) and 1 M, 2 M, 3 M and 4 M hydrogen peroxide solution (right to left). Scale bar: 1 cm. In all cases, a current density of −0.7 mA cm^{-2} was applied for 900 seconds. Conditions; Fmoc-3 = [5 mg mL^{-1}], NaCl = [0.1 M].

However, there were visible differences in the surface structure and smoothness of the resultant hydrogel films. Images of the hydrogel films in the absence of hydrogen peroxide and when 70 μL aliquots of 1, 2, 3 and 4 M solutions show that in the absence of hydrogen peroxide and at lower concentrations of hydrogen peroxide, the hydrogel film contains many holes where hydrogen gas bubbles have escaped through the material (Fig. 2g). As the Fmoc group is base labile, care must be taken to ensure that the high pH environment does not cleave the Fmoc group from the molecule to form dibenzofulvene.[21] To confirm that this does not occur during the electrodeposition process, ^{1}H NMR spectra of the freeze-dried gels were collected and compared with the spectra of the pure Fmoc-3 gelator (Fig. S4, ESI†). The spectra confirm that the Fmoc group does not cleave during the gelation process.

When the gelation process relies on the electrolysis of water, the gaseous by-products escape through the hydrogel on the electrode surface, leaving holes.[10,22] For most applications, material reproducibility and homogeneity are of the utmost importance. As the electrochemical reduction of water results in hydrogen bubble holes throughout the Fmoc-3 hydrogels, the fabrication process is unsuitable for the formation of reproducible hydrogels. The addition of hydrogen peroxide circumvents this issue; as the concentration of hydrogen peroxide is increased, the gelation process relies mostly on hydrogen peroxide reduction. This therefore results in fewer holes throughout the hydrogel to produce materials with smooth surfaces (Fig. 2g and Fig. S4, ESI†).

To investigate the effect of hydrogen peroxide concentration on the stiffness and breaking point of the gels, bulk rheology was used. Strain and frequency sweeps were performed on the Fmoc-3 hydrogels grown in the absence of hydrogen peroxide and across the full hydrogen peroxide concentration range (from 1 to 4 M), Fig. S9 (ESI†). For all the hydrogels, the storage modulus (G') and loss modulus (G'') values are similar (approximately $G' = 10^5$, $G'' = 10^4$ Pa). However, as the concentration of hydrogen peroxide is increased, the strain values become more reproducible between gels grown under the same conditions (Fig. 2a–e). The Fmoc-3 hydrogels grown in the presence of 70 μL of a 4 M hydrogen peroxide have the lowest errors in both G' and G'' (Fig. 2a–e and Fig. S9, ESI†), showing that a hydrogen peroxide concentration of 4 M is the optimal concentration for reproducible hydrogel formation.

At lower hydrogen peroxide concentrations, the holes created by gas bubbles make it difficult to image and accurately calculate gel volume so we only discuss data for when 70 μL of a 4 M H_2O_2 was added. To monitor the rate of gel growth, we measured the how the gel area changes with time for gels grown on a circular glassy carbon macroelectrode (Fig. S10, ESI†). By plotting gel area vs time graphs, we can confirm through linearity of this plot that growth is diffusion controlled and calculate the diffusion coefficient of the rate determining species diffusing from the electrode surface from the slope of this graph.[5] As well as this, when the area becomes invariant with time (zero slope) we can determine the final size of the hydrogel. Photographs of the hydrogels were taken *in situ* at 30 second intervals for 900 seconds (Fig. S6a, ESI†). The gel area, determined using ImageJ, Is confirmed to increase linearly with time up until 600 seconds after which the gel area plateaus. To determine whether the concentration of the Fmoc-3 hydrogel changes after this plateau point, quantitative ^{1}H NMR spectroscopy (qNMR) was used (Fig. S7, ESI†). The concentration of the Fmoc-3 within the hydrogels grown for 600 and 900 seconds is almost identical, indicating that in each case gel growth stops after this plateau point of around 600 seconds. To ensure that hydrogen peroxide depletion was not the limiting factor determining hydrogel growth, a second aliquot of hydrogen peroxide solution (a further 70 μL of a 4 M solution) was added at 600 seconds (gel growth plateau point), followed by further application of current for another 600 seconds. The qNMR results (Fig. S7, ESI†) show that there was no further increase in concentration, indicating this is a practical limit of gels growth.

It is notable that our previous studies using acid triggered gelation[5] did not result in a similar cessation of gel growth with time. We therefore postulate that this difference is due to the effective acid buffering provided by the diffusion of dissolved carbonic acid species from bulk solution to electrode at outside of the pH zone, where the pH excursion has become sufficiently small. To confirm this, when the pH of the gelator solutions was adjusted to pH 8 prior to deposition, effectively converting all dissolved carbonic acid to bicarbonate but with the solution pH still below the gelator pK_a, the gel area did not plateau after 300 seconds but rather continued to increase linearly with deposition time (Fig. S6b, ESI†). It is worth noting that further buffering is also possible through a second deprotonation of bicarbonate above pH $\sim$ 10.5, but this would still result in pH values that result in gelator deprotonation and gel formation. A larger gel was also formed as compared to the gel grown from the pH = 6.5 gelator solution. In this case, when the pH in the zone near the electrode is such that gel growth ''outruns'' buffer transport, and where the concentration of hydroxide ions is larger than that of the buffering species, we would expect the growth of this high pH zone to be governed by diffusion path length of these hydroxide ions. As previously for acid triggered growth, assuming three-dimensional diffusion-controlled growth of a near hemispherical gel for which $r^2 = 6Dt$, the diffusion coefficient is then calculated from the slope of the gel area vs time graphs to be 3.7×10^{-5} cm^2 s^{-1} at pH = 6.5 and 4.8×10^{-5} cm^2 s^{-1} at pH = 8 respectively. These values are reassuringly close to the expected diffusion coefficient for hydroxide ions in water ($D = 5 \times 10^{-5}$ cm^2 s^{-1}).[23] Fmoc-3 hydrogels changes at various concentrations of hydrogen peroxide, confocal microscopy images were taken of gels grown in the absence of hydrogen peroxide and gels grown across the full hydrogen peroxide concentration range (Fig. 3 and Fig. S5, ESI†). Despite presenting different surface smoothness and topography (Fig. 2g), all the Fmoc-3 hydrogels appear to have the same microstructure,

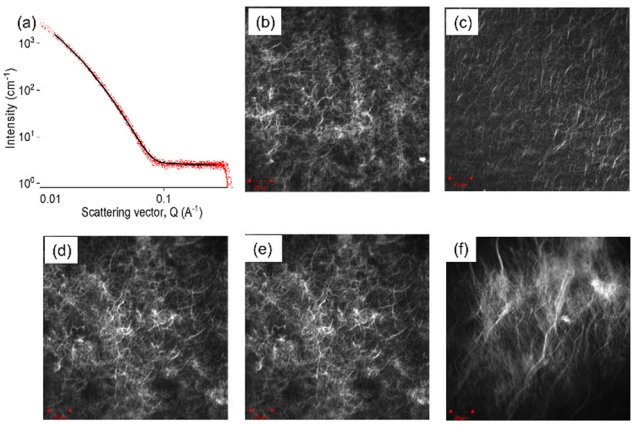

Fig. 3 (a) SAXS data and fit for Fmoc-3 hydrogels grown using 4 M hydrogen peroxide solution. Confocal microscopy images of Fmoc-3 hydrogels fabricated (b) in the absence of hydrogen peroxide and at various concentrations of hydrogen peroxide (c) 1 M (d) 2 M (e) 3 M (f) 4 M. For all, a current density of -0.7 mA cm^{-2} was applied for 900 seconds. Conditions; Fmoc-3 = [5 mg mL^{-1}], NaCl = [0.1 M].

exhibiting long fibers with a number of spherulitic domains (Fig. 3 and Fig. S5, ESI†). Notably, For the 4 M sample, the fibres appear to be longer in comparison to the other Fmoc-3 hydrogel microstructures as well as displaying a greater contrast with the solvent. The hydrogels formed in the presence of 4 M hydrogen peroxide solution contain few to no hydrogen bubble holes. It is therefore likely that the increase in contrast and fibre length are due to the increased homogeneity of the sample as the three-dimensional network is not disrupted by the gas bubbles. To examine the microstructure at different stages of the deposition process, confocal microscopy images were collected from gels grown for 300, 600 and 900 seconds (Fig. S5, ESI†). Again, in all cases, the images show that long fibres and a number of spherulitic domains are present. This suggests the microstructure remains the same throughout the deposition process. Multiple images were collected at various positions, confirming the microstructure was homogeneous throughout the material.

To probe the primary self-assembled structures of the Fmoc-3 hydrogels, small angle X-ray scattering (SAXS) was used (Fig. 3a and Fig. S11, ESI†). Full experimental details can be found in the ESI† (Section S10). SAXS data were collected from hydrogels grown in the absence of hydrogen peroxide and across the full hydrogen peroxide concentration range (adding aliquots of 1–4 M solutions). Fitting the SAXS data was carried out using SasView software.[24] Full fitting parameters for can be found in Table S2 (ESI†). In all cases, the SAXS data were best fit to a flexible elliptical cylinder model with a polydispersity in radius. Hydrogels grown in the absence of hydrogen peroxide display a Kuhn length and radius (minor axis) of 7.1 nm and 4.3 nm respectively. As the concentration of hydrogen peroxide is increased, the Kuhn length and radius gradually decrease. The Kuhn length represents the stiffness of the elliptical shaped cylinder structures; as the Kuhn length increases, the structures become less flexible and more rigid. There is no necessary link between radius and Kuhn length. A polydispersity of the radius was also used to fit the data. This indicates that there is a distribution of the radii of the structures. As the orientation of the Fmoc-3 molecules within the fibres is unknown, it is hard to make assumptions as to the expected dimensions of the fibres with respect to the molecular packing.

For hydrogels grown in the presence of 4 M hydrogen peroxide solution, the Kuhn length and radius are 4.9 nm and 3.5 nm respectively. The axis ratio increases with increasing hydrogen peroxide concentration from 5.95 (hydrogels grown in the absence of hydrogen peroxide) to 7.50 (4 M hydrogen peroxide solution). This suggests the self-assembled structures are more tape-like as the concentration of hydrogen peroxide is increased. For the 4 M sample, SAXS data were collected from hydrogels grown for 300 and 600 seconds to examine if deposition time effects the primary self-assembled structures. For the hydrogels grown for 300 and 600-seconds the SAXS data imply. that the radius and axis ratio values are similar. However, their Kuhn length values of 6.4 nm (300 s) and 6.9 (600 s) are higher than hydrogels grown for 900 seconds (4.8 nm), suggesting that the self-assembled structures are less flexible at shorter deposition times.

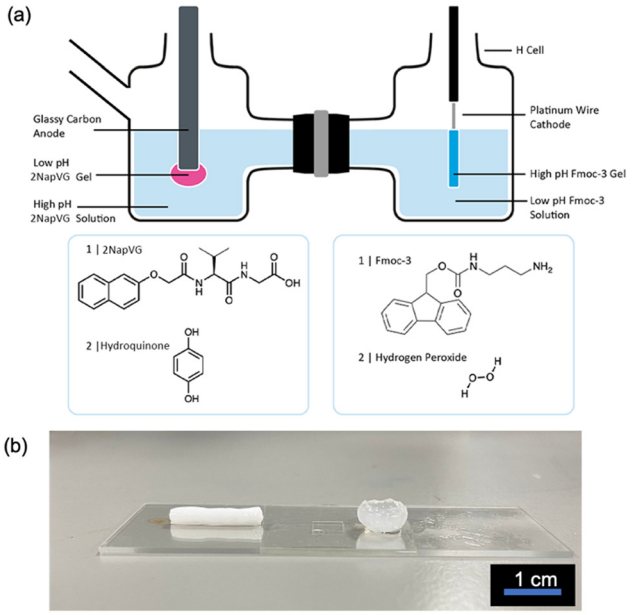

Fig. 4 (a) Schematic representation of the electrochemical system used to simultaneously grow two different hydrogels at opposing pH extremes (b) Images of the 2NapVG (right) and Fmoc-3 (left) hydrogels grown using this technique. A current density of 22 mA cm^{-2} was applied for 900 seconds. Scale bar: 1 cm. Initial reaction conditions; Fmoc-3 = [5 mg mL^{-1}], NaCl = [0.1 M], H_2O_2 = [200 μL, 4M], 2Nap-VG-OH = [5 mg mL^{-1}], hydroquinone [5 mg mL^{-1}], NaCl = [0.1 M], pH = [8].

This system can be coupled with an acid triggered LMWG to form two hydrogels at opposing pH extremes simultaneously on electrode surfaces (Fig. 4). Previously, we have shown that naphthalene-protected dipeptide gelators such as 2NapVG can form gels *via* the electrochemical oxidation of hydroquinone which results in a local pH decrease at the electrode surface.[5,13,15] To couple both of these methods, a custom-made H-cell (Fig. 4a and Fig. S12, ESI†) was employed, consisting of two glass chambers separated by a Nafion membrane.

In one chamber, the working electrode (glassy carbon) and reference electrode (Ag/AgCl) was placed in a 2NapVG and hydroquinone solution. In the other chamber, the counter electrode (platinum wire) was placed in an Fmoc-3 and hydrogen peroxide solution. To simultaneously grow the Fmoc-3 and 2NapVG hydrogels, a current density of 22 mA cm^{-2} was applied to the working electrode for 900 seconds. Upon application of the current, hydrogel formation was observed on both the working and counter electrode surface in their respective chambers (Fig. 4b). The application of an anodic current to the working electrode in the right-hand side chamber sees the oxidation of hydroquinone to benzoquinone, liberating protons at the electrode-solution interface. This localised decrease in pH triggers the 2NapVG molecules to self-assemble and form a hydrogel exclusively at the electrode surface.[5,15] To complete the electrochemical circuit, the hydrogen peroxide in the second chamber is reduced at the counter electrode, generating hydroxide ions, resulting in self-assembly of Fmoc-3 and gel formation on the counter electrode. Consequently, low pH hydrogels of 2NapVG are formed on the working electrode surface (anode) and high pH

hydrogels of Fmoc-3 are formed on the counter electrode surface (cathode).

In conclusion, we have shown that we can electrochemically form hydrogels at high pH, with the gel properties being greatly improved by the addition of hydrogen peroxide. This system can be coupled with acid-triggered gelators to form two hydrogels triggered at opposing pH extremes simultaneously in a spatially and temporally controlled manner.

Conflicts of interest

There are no conflicts to declare.

Acknowledgements

CP and DA thank the Leverhulme Trust for funding (RPG-2019-165).

References

1 J. Zhuang, S. Lin, L. Dong, K. Cheng and W. Weng, Magnetically Assisted Electrodeposition of Aligned Collagen Coatings, *ACS Biomater. Sci. Eng.*, 2018, **4**, 1528–1535.
2 J. Li, S. Wu, E. Kim, K. Yan, H. Liu, C. Liu, H. Dong, X. Qu, X. Shi, J. Shen, W. E. Bentley and G. F. Payne, Electrobiofabrication: electrically based fabrication with biologically derived materials, *Biofabrication*, 2019, **11**, 032002.
3 Z. Yang, Z. Yuye, L. Houbin, D. Fuyuan and S. Xiaowen, Electrodeposition of Polysaccharide and Protein Hydrogels for Biomedical Applications, *Curr. Med. Chem.*, 2019, **26**, 1–21.
4 K. Sipa, K. Kowalewska, A. Leniart, A. Walcarius, G. Herzog, S. Skrzypek and L. Poltorak, Electrochemically assisted polyamide deposition at three-phase junction, *Electrochem. Commun.*, 2021, **123**, 106910.
5 C. Patterson, B. Dietrich, C. Wilson, A. R. Mount and D. J. Adams, Electrofabrication of large volume di- and tripeptide hydrogels via hydroquinone oxidation, *Soft Matter*, 2022, **18**, 1064–1070.
6 Y. Liu, E. Kim, R. V. Ulijn, W. E. Bentley and G. F. Payne, Reversible Electroaddressing of Self-assembling Amino-Acid Conjugates, *Adv. Funct. Mater.*, 2011, **21**, 1575–1580.
7 M. Lei, X. Qu, H. Wan, D. Jin, S. Wang, Z. Zhao, M. Yin, F. Payne Gregory and C. Liu, Electro-assembly of a dynamically adaptive molten fibril state for collagen, *Sci. Adv.*, 2022, **8**, eabl7506.
8 S. Wu, K. Yan, J. Li, R. N. Huynh, C. B. Raub, J. Shen, X. Shi and G. F. Payne, Electrical cuing of chitosan's mesoscale organization, *React. Funct. Pol.*, 2020, **148**, 104492.
9 X. Qu, H. Liu, C. Zhang, Y. Lei, M. Lei, M. Xu, D. Jin, P. Li, M. Yin, G. F. Payne and C. Liu, Electrofabrication of functional materials: Chloramine-based antimicrobial film for infectious wound treatment, *Acta Biomater.*, 2018, **73**, 190–203.
10 J. E. Bressner, B. Marelli, G. Qin, L. E. Klinker, Y. Zhang, D. L. Kaplan and F. G. Omenetto, Rapid fabrication of silk films with controlled architectures via electrogelation, *J. Mater. Chem. B*, 2014, **2**, 4983–4987.
11 F. Ozawa, K. Ino, T. Arai, J. Ramón-Azcón, Y. Takahashi, H. Shiku and T. Matsue, Alginate gel microwell arrays using electrodeposition for three-dimensional cell culture, *Lab Chip*, 2013, **13**, 3128–3135.
12 A. Gargava, S. Ahn, W. E. Bentley and S. R. Raghavan, Rapid Electroformation of Biopolymer Gels in Prescribed Shapes and Patterns: A Simpler Alternative to 3-D Printing, *ACS Appl. Mater. Interfaces*, 2019, **11**, 37103–37111.
13 E. K. Johnson, D. J. Adams and P. J. Cameron, Directed Self-Assembly of Dipeptides to Form Ultrathin Hydrogel Membranes, *J. Am. Chem. Soc.*, 2010, **132**, 5130–5136.
14 M. Lei, X. Qu, H. Liu, Y. Liu, S. Wang, S. Wu, W. E. Bentley, G. F. Payne and C. Liu, Programmable Electrofabrication of Porous Janus Films with Tunable Janus Balance for Anisotropic Cell Guidance and Tissue Regeneration, *Adv. Funct. Mater.*, 2019, **29**, 1900065.
15 J. Raeburn, B. Alston, J. Kroeger, T. O. McDonald, J. R. Howse, P. J. Cameron and D. J. Adams, Electrochemically-triggered spatially and temporally resolved multi-component gels, *Mater. Horiz.*, 2014, **1**, 241–246.
16 V. Lakshminarayanan, L. Poltorak, E. J. R. Sudhölter, E. Mendes and J. van Esch, Electrochemically assisted hydrogel deposition, shaping and detachment, *Electrochim. Acta*, 2020, **350**, 136352.
17 R. A. Zangmeister, J. J. Park, G. W. Rubloff and M. J. Tarlov, Electrochemical study of chitosan films deposited from solution at reducing potentials, *Electrochim. Acta*, 2006, **51**, 5324–5333.
18 S. Selmani, E. Schwartz, J. T. Mulvey, H. Wei, A. Grosvirt-Dramen, W. Gibson, A. I. Hochbaum, J. P. Patterson, R. Ragan and Z. Guan, Electrically Fueled Active Supramolecular Materials, *J. Am. Chem. Soc.*, 2022, **144**, 7844–7851.
19 S. Panja and D. J. Adams, Maintaining homogeneity during a sol–gel transition by an autocatalytic enzyme reaction, *Chem. Commun.*, 2019, **55**, 47–50.
20 D. Pines, J. Ditkovich, T. Mukra, Y. Miller, P. M. Kiefer, S. Daschakraborty, J. T. Hynes and E. Pines, How Acidic Is Carbonic Acid?, *J. Phys. Chem. B*, 2016, **120**, 2440–2451.
21 D. A. Wellings and E. Atherton, *Methods in Enzymology*, Academic Press, 1997, vol. 289, pp. 44–67.
22 G. G. Leisk, T. J. Lo, T. Yucel, Q. Lu and D. L. Kaplan, Electrogelation for Protein Adhesives, *Adv. Mater.*, 2010, **22**, 711–715.
23 S. Takai, S. Murakami, L. Zhang, K. Ohsasa and S. Watanabe, Quantitative Evaluation of the Diffusion Coefficients of Aqua Ions in Hydrogels via Iron Corrosion, *ACS Appl. Eng. Mater.*, 2023, **1**, 80–86.
24 SasView, **http://www.sasview.org/**.